HHS Public Access

Author manuscript

Nat Immunol. Author manuscript; available in PMC 2017 November 22.

Published in final edited form as:

Nat Immunol. 2017 July ; 18(7): 771–779. doi:10.1038/ni.3751.

CD8αα$^+$ Intraepithelial Lymphocytes Arise from Two Major Thymic Precursors

Roland Ruscher[1], **Rebecca L. Kummer**[1], **You Jeong Lee**[2], **Stephen C. Jameson**[1], and **Kristin A. Hogquist**[1]

[1]The Department of Laboratory Medicine and Pathology and Center for Immunology, University of Minnesota, Minneapolis, Minnesota USA

[2]Academy of Immunology and Microbiology, Institute for Basic Science (IBS), and Division of Integrative Biosciences and Biotechnology, Pohang University of Science and Technology (POSTECH), Pohang, Republic of Korea

Abstract

TCRαβ$^+$ CD8αα$^+$ intestinal intraepithelial lymphocytes (CD8αα IELs) are an abundant population of thymus-derived T cells that protect the gut barrier surface. We sought to better define the thymic IEL precursor (IELp) by analysis of their maturation, localization, and emigration. We defined two precursors among TCRβ$^+$CD4$^-$CD8$^-$ thymocytes using TAK1 dependence and rigorous lineage-exclusion criteria. Those IELp populations include a nascent PD-1$^+$ population and a T-bet$^+$ population that accumulated with age. Both gave rise to intestinal CD8αα IELs upon adoptive transfer. PD-1$^+$ cells contained more strongly self-reactive clones and were largely classical MHC restricted. They localized to the cortex, and efficiently emigrated in an S1PR1-dependent manner. T-bet$^+$ IELp localized to the medulla, included non-classical MHC-restricted cells and expressed NK1.1, CD103 and CXCR3. The two IELp populations further differed in TCR V_α and V_β usage. These data provide an important foundation for understanding the biology of CD8αα IELs.

Introduction

Intestinal intraepithelial lymphocytes (IELs) are a heterogeneous T cell population embedded within the intestinal epithelial layer, where they carry out numerous effector, regulatory and protective functions[1,2]. How IELs exert these functions is not fully understood. IELs include memory TCRβ$^+$CD4$^+$ and TCRβ$^+$CD8αβ$^+$ cells generated from naive T cells during an immune response (induced IELs), and TCRγδ$^+$ and TCRβ$^+$CD8α$^+$CD8β$^-$ (CD8αα IELs) cells that differentiate in the thymus (natural IELs)[2].

Correspondence should be addressed to K.A.H. (hogqu001@umn.edu).

Author Contributions: R.R. and K.A.H. designed experiments; R.R., R.L.K. and Y.J.L. performed experiments and analyzed data; R.R. wrote the manuscript; S.C.J. provided input for interpretation; K.A.H. conceptualized and directed the study, and edited the manuscript.

Competing Financial Interests: The authors have no competing financial interests.

The development of natural CD8αα IELs has been the subject of extensive research, yet the precise thymic precursor remained enigmatic. Post-selection IEL precursors (IELp) can be found within the double-negative (DN) thymocyte population as CD5 and TCRβ expressing cells[3-5], although within this population, there is still substantial heterogeneity. Various molecules including T-bet, PD-1, integrin $\alpha_4\beta_7$ and CD103 have been implicated in IEL development[4-7]. Yet further features of IEL development are not yet known, including localization, emigration patterns and TCR specificity. Recent approaches suggested variability in MHC-restriction amongst CD8αα IELs[4,5].

Previous studies on IELp relied on NK1.1 as an exclusion marker for invariant NKT cells (iNKTs). This approach however does not exclude thymic iNKT subsets that are NK1.1^{-}, namely NKT2 and NKT17 cells[8]. Here, we investigated thymic IELp development and emigration in detail, using a CD1d-tetramer (CD1dtet) to specifically exclude iNKT cells. We discovered two distinct mature DN T cell subsets of different phenotype, which can differentiate into CD8αα IELs. One was PD-1^{+} and enriched in self-reactive cells, confirming in the polyclonal setting what had previously been found in a retrogenic model[5]. The second subset was a previously unrecognized PD-1^{-} T-bet^{+} population that highly expressed NK1.1. This population did not show signs of overt self-reactivity compared to the PD-1^{+} population, and included non-classical class I-restricted cells. The two subsets further differed in TCRα- and TCRβ-chain usage, and had different thymic emigration behavior. Even though T-bet^{+} IELp had a more mature “IEL-like” phenotype, the major emigrating IELp cells were PD-1^{+} and expressed $\alpha_4\beta_7$ integrin. Both IELp were able to seed the gut, where they expressed CD8αα, and since the PD-1^{+} IELp downregulated PD-1 and increased T-bet expression, cells arising from the two progenitors were largely indistinguishable in the gut environment using conventional markers. Our study reconciles variability in phenotypes and MHC restriction reported for IELp, in addition to revealing novel aspects of IELp development and functionality.

Results

Thymic TCRβ^{+}DN Cells Contain a Mature IELp Population

Previous data suggested that IELp could be found with the TCRβ^{+}CD5^{+}CD4^{-}CD8^{-} DN gate[3,5]. We used this gating strategy and further excluded iNKT cells (using a CD1dtet loaded with the cognate antigen analogue PBS57) and CD25^{+} regulatory T cells (Fig. 1a). Within this DN population, approximately one-third showed a mature phenotype, as evidenced by increased H-2K^{b} expression[9] and CD122 was highly expressed by H-2K^{b+} cells (Fig. 1b). TCRβ^{+} mature T cells require the kinase TAK1 for maturation[9]. Analysis of *Tak1*$^{fl/fl}$*Cd4*^{Cre} mice confirmed the selective absence CD8αα IELs, but not TCRγδ^{+} IELs in the small intestine (Fig. 1c), as previously reported[10]. Correspondingly, we observed a reduction of CD122^{+}H-2K^{b+} DN thymocytes in TAK1-deficient mice (Fig. 1b), suggesting this population represents mature precursors. Wild-type mature CD122^{+}(H-2K^{b+}) cells within total CD5^{+}TCRβ^{+} DN also showed little CD69 expression (Fig. 1d), analogous to mature conventional thymocytes. These results indicate that within the CD25^{-}CD1dtet^{-}CD5^{+}TCRβ^{+} DN population, mature cells, including mature IELp, can be

identified as CD122^{+}H-2K^{b+} cells. This gating strategy for mature IELp has been applied throughout the remainder of the manuscript, unless denoted otherwise.

Mature TCRβ^{+}DN Cells Divide into Two Major Subsets

We reasoned that within the mature DN population, IELp might express molecules critical for CD8αα IEL development, such as the transcription factor T-bet[6]. Within the mature TCRβ^{+} DN population of T-bet–green fluorescent protein (GFP) reporter mice (*Tbx21*^{GFP}), distinct GFP^{-} and GFP^{hi} cells were present (Fig. 2a). IELs were suggested to arise from precursors diverted from clonal deletion in response to strong TCR signaling[5,11,12]. PD-1 is upregulated by TCR signaling, and was previously shown to be expressed on DN thymocytes in mice expressing retrogenic IEL T cell receptors[5]. Interestingly, only the DN cells lacking T-bet expressed abundant PD-1 (Fig. 2b). Furthermore, in *Nr4a1*^{GFP} (Nur77^{GFP}) reporter mice, only the PD-1^{+} cells exhibited high expression of GFP, which indicates recent and strong TCR stimulation (Fig. 2b). Consistent with clonal deletion being an alternate fate for IELp, the percentage and number of PD-1^{+} DN cells was increased 35-fold in the thymus of *Bim*$^{-/-}$ mice (Fig. 2c), a model where normally deleted T cells are rescued[13]. It is possible that PD-1^{+} cells are precursors to PD-1^{-}T-bet^{+} cells, and had only transiently experienced strong TCR signals prior to upregulating T-bet. Although PD-1^{-} mature DN cells were increased in *Bim*$^{-/-}$ mice, the fold change was much less than for the PD-1^{+} population. In addition, in *Cd28*$^{-/-}$ mice, in which self-reactive thymocytes are diverted into the CD8αα lineage[11], only PD-1^{+} but not PD-1^{-} mature DN were increased (Fig. 2d). These characteristics suggested that the PD-1^{+}(T-bet^{-}) and PD-1^{-}(T-bet^{+}) cells might represent separate lineages, and thus are referred to as “type A” and “type B” IELp, respectively, throughout the rest of the paper.

The integrins $\alpha_4\beta_7$ and α_E (also known as CD103) have been associated with gut homing and retention[14-16], thus we examined expression of these molecules on thymic progenitors. Type A cells were the predominant $\alpha_4\beta_7$-expressing cells, while only type B cells expressed CD103 (Fig. 2e). As T-bet expression in the thymus is high in *i*NKT cells[8,17], we also tested for other NKT-related molecules. Indeed type B but not type A cells were NK1.1^{+} (Fig. 2f), although they did not bind CD1dtet. Type B cells also expressed yellow fluorescent protein (YFP) in *Ifng*^{YFP} reporter mice (Fig. 2g).

To further explore whether type A and B cells represent distinct progenitors, we employed spanning tree analysis[18,19] with an extended marker panel. All TCRβ^{hi} (post-selection) thymocytes were included in the analysis, and major clusters of CD4^{+}CD8^{+} double-positive (DP), mature CD4SP and mature CD8SP are denoted (Fig. 2h and Supplementary Fig. 1a-l). A cluster of *Tbx21*$^{GFP+}$ cells was located off the CD4SP branch, which included CD1dtet-binding *i*NKT cells, but contained two nodes of CD1dtet^{-} cells matching the type B phenotype (Fig. 2h,j and Supplementary Fig. 1b-i). In contrast, the only nodes corresponding to type A cells emerged near the DP progenitor group (Fig. 2h,j and Supplementary Fig. 1b-i). Enumeration revealed a similar ratio of type A to B cells as found in the total thymus by our flow gating strategy (Fig. 2a,i). We furthermore found CD44 and CXCR3 to be expressed by type B but not type A cells (Fig. 2j and Supplementary Fig. 1j,l). Both types were negative for CCR7 (Fig. 2j and Supplementary Fig. 1k), a chemokine receptor

associated with migration of developing T cells from the thymic cortex to the medulla[20,21]. In conclusion we identified two main subtypes within the mature TCRβ$^+$DN cells distinguished by expression of PD-1, or T-bet and NK1.1.

Both Type A and B Cells Give Rise to CD8αα IELs

To determine the capacity of each mature DN subtype to develop into CD8αα IELs, we adoptively transferred sorted type A or B cells together with congenically different total CD4$^-$CD8$^-$ DN control thymocytes into *Rag2*$^{-/-}$ recipients and recovered the cells from spleen and small intestine IEL 5-10 weeks later. While TCRβ$^+$ control competitors gave rise to heterogeneous CD4$^+$ and CD8$^+$ cells in both the IEL compartment as well as the spleen, virtually all type A and B cells gave rise exclusively to CD8αα$^+$ IEL in the intestine (Fig. 3a and Supplementary Fig. 2a). This strong fate determination was tissue-specific as CD8αα$^+$ descendants of either IELp subset were not significantly enriched in the spleen (Supplementary Fig. 2b). A and B cells competed equivalently with the controls cells, and experiments in which type A IELp were transferred together with type B IELp resulted in similar outcomes (data not shown), suggesting that both progenitors have robust potential to seed the gut, at least in *Rag2*$^{-/-}$ recipients.

Type A IELp Are Nascent While B Accumulate With Age

CD103 expression is not only associated with IELs and IELp[2,6] but also with tissue-resident T cells[22]. We were therefore interested in determining if type B IELp are retained in the thymus. To do so, we made use of *Rag2*^{GFP} mice, in which GFP is highly expressed in thymocytes at the DP stage and degrades over time after positive selection[23,24]. While type A IELp exhibited similar *Rag2*^{GFP} expression to developing CD4SP thymocytes, type B IELp were *Rag2*$^{GFP-}$ (Fig. 3b), suggesting that the latter population is older, or had proliferated extensively. As GFP abundance would be diluted by proliferation, we tested cell cycle activity by Ki-67. Type B IELp had strongly reduced Ki-67 expression (Fig. 3c), indicating that depleted GFP was not due to recent proliferation. In addition, the maturation marker Qa2 was highly expressed on type B IELp with intensity far exceeding those of type A IELp (Fig. 3d). Furthermore, while the absolute number of type A IELp declined, the type B population accumulated with the age of mice (Fig. 3e). Of note, these findings were not due to recirculation of type B cells as indicated by adoptive transfer and parabiosis studies (not shown). In summary, type A IELp appear to be developmentally younger than type B IELp, with the latter expressing markers indicative of thymic retention. Nevertheless both types, once in circulation, have an inherent capacity to seed an open niche and become CD8αα$^+$ IELs.

Type A and B IELp Localize Differently in the Thymus

CXCR4 and CCR9 are predominantly expressed by DP thymocytes and are thought to be involved in their cortical localization[25-27]. On the other hand, CCR4 and CCR7 expression are induced upon positive selection and associated with thymocyte migration from the cortex to the medulla[20,21,26,28]. Both IELp types were devoid of surface CCR9 and were negative or low for CXCR4 (Fig. 4a), consistent with their post-selection maturation status. However, neither IELp expressed CCR4 or CCR7. CXCR3 expression has been suggested to retain *i*NKT cells in the medulla[29]. Type B were CXCR3$^+$, consistent with our SPADE-analysis

results, but type A IELp were not. Given these patterns, it is not easy to predict where each precursor would be localized within the thymus.

To directly test this, we devised an immunofluorescence staining strategy. Flow cytometry-based backgating showed that within total thymocytes, PD-1^{hi}*Nr4a1*^{GFPhi} cells were predominantly CD5^{+}TCRβ^{+} DN (Supplementary Fig. 3a). Total *Tbx21*^{GFPhi}CD1dtet$^{–}$ thymocytes were largely CD5^{+}TCRβ^{+} DN which contained mainly mature type B IELp (Supplementary Fig. 3b). Thus, we employed immunofluorescence-based quantitative histo-cytometry[30] using these markers to determine the thymic localization of type A and type B IELp. Comparing flow cytometry to quantitative immunofluorescence revealed a higher proportion of both IELp types by imaging as compared to flow cytometry (Fig. 4b,e). This is in agreement with a previous publication reporting that cell isolation and flow cytometry can underestimate T cell numbers[31]. We next quantified the localization of gated events: 70% of PD-1^{hi}*Nr4a1*^{GFPhi} (type A) cells were in the cortex, while the remaining 30% were typically in the cortico-medullary junction (Fig. 4b-d and not shown). In contrast, 75% of *Tbx21*^{GFPhi}CD1dtet$^{–}$ (type B) cells could be found in the medulla (Fig. 4e-g).

As interleukin 15 (IL-15) is a cytokine that can induce T-bet expression[6], and *i*NKT cells in the thymus were suggested to depend on medullary thymic epithelial cell (mTEC)-derived IL-15–IL15Rα[32], we tested the effects of IL-15 deficiency on IELp. Type B IELp were found to be depleted in lethally irradiated *Il15*$^{-/-}$ mice reconstituted with *Tbx21*^{GFP} bone marrow cells, while type A IELp were still present (Supplementary Fig. 3c). Interestingly, CD122 expression by mature IELp was not affected in *Il15*$^{-/-}$ chimeras (Supplementary Fig. 3c). These results suggest a preferential cortical versus medullary thymic localization of type A or B IELp, respectively.

Emigration of Type A IELp Is Dominant over Type B IELp

We next investigated the emigrational properties of IELp. Thymic emigration of conventional T cells and IELp is mediated by S1PR1 targeted by the transcription factor KLF2 (refs. [33-35]). Within the mature IELp population 15% were *Klf2*$^{GFP+}$S1PR1^{+} (Supplementary Fig. 4a). Reciprocally, most of the *Klf2*$^{GFP+}$S1PR1^{+} cells among total CD4$^{–}$CD8α$^{–}$CD5^{+}TCRβ^{+} IELp were CD122^{+}H-2K^{b+} (Supplementary Fig. 4b). The *Klf2*$^{GFP+}$S1PR1^{+} mature IELp population contained mainly type A cells, which had a significantly higher proportion of $\alpha_4\beta_7^{+}$ cells as compared to the total mature type A IELp (Fig. 5a). This suggests that type A IELp express $\alpha_4\beta_7$ as they become emigration-competent.

Intravenous labeling with CD45-phycoerythrin has previously been used to define CD4SP thymocytes that are emigrating, as they are thought to do so from perivascular spaces (PVS) at the cortico-medullary boundary[36]. We employed this technique for IELp and found that in the labeled fraction, type A IELp were more abundant than type B IELp, and even further enriched as compared to the unlabeled parenchymal IELp (Fig. 5b).

In a further approach, we defined peripheral recent thymic emigrants (RTE) using ultrasound-guided intrathymic biotin-labeling (Supplementary Fig. 5a) and analysis of streptavidin^{+} cells in the spleen 24 hours later (Supplementary Fig. 5b). Within the splenic

RTEs, type A cells were enriched compared to their proportion in the thymus tissue (Fig. 5c), which is in agreement with the type A enrichment in the labeled fraction (Fig. 5b). On the contrary, type B cells were reduced in RTEs when compared with their proportion in the thymus tissue (Fig. 5c).

To determine if type A IELp emigrate in an S1PR1-dependent fashion, we treated *Rag2*^{GFP} mice with the S1PR1 functional antagonist FTY720 for six consecutive days. The percentage of GFP$^+$ splenic CD1dtet$^-$CD25$^-$TCRβ$^+$ cells was strongly reduced, as expected (Supplementary Fig. 5c). DN cells within this fraction were almost entirely depleted of mature-phenotype IELp (Supplementary Fig. 5c). Of note, the mature IELp cells in untreated mice were predominantly PD-1$^+$α$_4$β$_7^+$ (Supplementary Fig. 5c), consistent with the enrichment of these cells in the *Klf2*$^{GFP+}$S1PR1$^+$ compartment of mature IELp. These results suggest that type A IELp are the main population exiting the thymus in the steady state, and their emigration is S1PR1-dependent. However our data also indicate that despite being retained in the thymus, a small fraction of type B IELp also emigrates.

Type B Do Not Arise from Type A IELp

We analyzed IELp in FTY720-treated mice to investigate the effects of retention on their phenotype. Interestingly, type A IELp trapped in the thymus with FTY720 treatment gradually lost their PD-1 surface expression and began to express *Tbx21*^{GFP} (Supplementary Fig. 6a). Bin gating on PD-1^{hi} (gate 1), PD-1^{int} (gate 2), PD-1^{lo} (gate 3) and PD-1$^-$ (gate 4) mature IELp revealed an increase in numbers in all these stages (Supplementary Fig. 6a). Interestingly, we also found an increase in α$_4$β$_7$ expression in the PD-1^{int}, PD-1^{lo} and PD-1$^-$ stages (Supplementary Fig. 6b), consistent with the accumulation of a trapped type A population that begins to differentiate toward a type B phenotype. However, the population of *Tbx21*^{GFPhi} type B IELp remained α$_4$β$_7^-$ and constant in numbers in spite of FTY720 administration for 6 days (Supplementary Fig. 6a, c).

To investigate the possibility of an immediate precursor-product relationship between type A and B IELp more rigorously, we performed “time-stamp” experiments. For this purpose we crossed *Cd4*^{CreERT2} with *Rosa26*^{TdT} (stop-floxed tdTomato) reporter mice. In these mice, tamoxifen will permanently label every DP or CD4$^+$ cell at the time of exposure. Although neither type A or B IELp express CD4, they are both derived from DP progenitors (data not shown). Therefore this approach allows the labeling of a cohort of DP progenitors and tracking through differentiation thereafter. Upon intraperitoneal tamoxifen administration, tdTomato expression was detected only in DP thymocytes on day 2, but was present in CD8SP on day 5 (Fig. 6a,b). Similar to CD8SP, type A IELp displayed a peak of tdTomato$^+$ cells 5 days after tamoxifen that was reduced 10 days after tamoxifen, consistent with emigration of these populations. No tdTomato$^+$ cells were found in the type B pool, which would be expected if type A cells differentiated into type B cells. Taken together, while type A IELp can downregulate PD-1 and express *Tbx21*^{GFP} when forcibly retained in the thymus, these cells do not contribute substantially to the type B IELp pool in the steady state.

Differential Antigen-Receptor Specificities in IELp Types

We were interested in finding out more about potential functional properties of type A versus B IELp. Investigating a small number of clones in retrogenic mice, it has been established that CD8αα IELs can be restricted by various MHC classes[4,5]. Similarly to previous publications[11,37], we found that IELs were strongly reduced in *B2m*$^{-/-}$ mice (Fig. 7a, left). This was recapitulated by a reduction in both type A and B IELp thymocytes (Fig. 7a, right), although the fold reduction was much larger in the gut than in the thymus (100 fold versus 5-6 fold). Conversely, only type A IELp were affected by deficiency in the classical MHC molecules H2-K^{b} and H2-D^{b} (Fig. 7a), consistent with type B IELp being restricted by non-classical Class I molecules. Type B IELp numbers (even when gated exclusively on PD-1^{+}NK1.1^{+}) were also lower in *Cd1*$^{-/-}$ mice, which lack expression of CD1d (Fig. 7b), suggesting the existence of type 2 NKT cells within this population. I-A^{b} deficiency did not significantly affect type A IELp but slightly diminished the number of type B IELp (Fig. 7c). Taken together, our data suggest differential MHC-restriction of type A versus B IELp and indicate greater involvement of β2m-dependent molecules in IEL maintenance in the gut, compared to selection in the thymus.

In addition to differential MHC dependence, the two IELp types also varied in TCR alpha chain usage: Comparing $V_{\alpha}2$ and $V_{\alpha}3.2$, type A IELp were highest in $V_{\alpha}2$ usage, while type B IELp were dominated by $V_{\alpha}3.2$ expression (Fig. 7d). Interestingly, the proportions of both $V_{\alpha}2^{+}$ and $V_{\alpha}3.2^{+}$ IEL were intermediate between those of thymic type A and B IELp (Fig. 7d). Given the lower thymic output of type B IELp this may reflect either stronger expansion of $V_{\alpha}3.2$ within the gut or stronger capacity of type B IELp to seed the IEL niche despite their absence of $\alpha_4\beta_7$. The V_{β} repertoire of type A and B IELp was also investigated. Of 14 analyzed V_{β} chains we found significantly reduced $V_{\beta}5.1/5.2$ and Vβ9, and significantly increased $V_{\beta}6$ in type B IELp (Supplementary Fig. 7). Taken together, in addition to phenotypic differences, type A and B IELp also vary in their MHC dependence and TCR usage, suggesting distinct antigen-specificities and potential function of the two subtypes.

Discussion

Thymic precursors of intestinal CD8αα IELs and their maturation, localization, and emigration are not fully characterized. In this study, we investigated these parameters and provided detailed analysis to this end. Our findings suggest the existence of two distinct subsets of mature IELp, which we termed “type A” and “type B” IELp. Type A IELp were localized in the cortex, and showed signs of strong agonist signaling. Thus, they have the expected characteristics of cells undergoing “clonal diversion” at the DP stage. In contrast, type B IELp reside in the medulla and contain few or no self-reactive cells. The majority of type B IELp cells were NK1.1^{+}, and would have been excluded from analysis in previous publications that used NK1.1 as an exclusion marker. Our data support a model in which in addition to the “mainstream” type A IELp, type B IELp with potentially different antigen specificity and function diversify the gut IEL repertoire.

In terms of the developmental relationship, we considered the possibility that type B IELp derived from type A IELp. However, the rescue of type A, but not B, IELp in Bim$^{-/-}$ and in

Cd28$^{-/-}$ mice, as well as the distinct TCR usage and MHC dependence, argue against this. Though we cannot exclude that a proportion of type B cells might have derived from cells in the type A pool, we favor the idea that the majority of type A and B IELp are on parallel rather than linear developmental pathways, as further supported by our time stamp experiments. Concordantly, SPADE analysis placed type B IELp into closer relation with CD4SP and iNKT cells, while type A IELp branched off from the DP pool. Our data also showed a differential impact of MHC deficiency on IELp. Type A IELp numbers were most affected by classic MHC class-I and β2m deficiency, while Type B IELp numbers were affected by MHC class-II, CD1d, and β2m deficiency. These findings are in line with recent reports that showed various classical and non-classical MHC molecule restriction by individual retrogenic systems IEL clones[4,5]. Due to a lack of specific markers on IEL derived from type A and type B precursors, we were unable to determine the relative proportion of gut resident lymphocytes derived from each. However, TCR V_α usage was distinct between type A and B thymic precursors, and intermediate amongst IEL suggesting that progeny of both are present in the gut.

The thymic localization and emigration versus retention properties of the two precursors was clearly distinct. About 25-30% of type A IELp cells were localized in proximity to the cortico-medullary junction, and we think it likely that these cortico-medullary IELp are about to emigrate from the thymus, similarly to conventional T cells[36]. How type B IELp, which are CCR4$^-$ and CCR7$^-$, migrate towards and are retained in the medulla is not clear. We considered the possibility that similarly to iNKT cells[29] CXCR3$^+$ type B IELp are retained by mTEC-derived CXCR3 ligands. However, we did not find differences in type A or B IELp proportions in CXCR3$^{-/-}$ compared to wildtype littermates (not shown). In addition, medullary IL-15 might play a role: In agreement with a study showing that IEL can develop without thymic IL-15[38], type B but not A IELp were strongly reduced in IL-15$^{-/-}$ chimeras. It is therefore possible that type B IELp accumulate in the medulla due to their dependence on IL-15. Type B IELp are similar to NKT1 in that they are IL-15-dependent, T-bet$^+$, CD44^{hi}, CXCR3$^+$, IFN-γ$^+$, are largely retained in the thymus and also preferentially localize to the medulla[8,17]. This similarity infers a mutual, albeit unidentified, function in the thymus. Intriguingly, differential MHC restriction and thymic localization also imply selection by different cell types rather than one specific APC. These aspects will be interesting to explore further in future studies.

S1PR1 expression, under the control of the transcription factor KLF2, has been established as a critical factor for emigration of conventional T cells[33,34]. While the contribution of S1PR1 in IELp trafficking from thymus to gut has been previously investigated[35,39], its involvement specifically in IELp egress from the thymus was controversial. Our findings suggest that type A IELp require this molecule for exiting the thymus. Of note, S1PR1$^+$ type A IELp and RTE were further enriched for $\alpha_4\beta_7$ expressing cells promoting mucosal tissue homing[14,15]. Indeed the complete absence of type A IELp in the spleen in animals treated for 6 days with an S1PR1 antagonist indicates swift parking in the gut and possibly other mucosal sites, or death, rather than extended circulation. Although we did not investigate this aspect for the minor emigrating type B IELp, they may have the same S1PR1 dependent mechanism for thymic exit.

In summary, we have identified two subsets of mature thymocytes distinguished by phenotype, TCR specificity and MHC-restriction, which we termed type A and type B IELp. Both can give rise to CD8αα small intestinal IELs. Given these disparities, functional differences between type A and B IELp are likely. Thus the findings of this study critically impact future expression profiling studies, understanding the roles of IEL in homeostasis and immunity, and how they relate to human IEL populations.

Methods

Mice

C57BL/6 (B6) and B6.SJL mice were purchased from the National Cancer Institute. *Tak1*$^{fl/fl}$, *Tak1*$^{fl/fl}$*Cd4*^{Cre}, *Tbx21*^{GFP} (T-bet^{GFP}), *Nr4a1*^{GFP} (Nur77^{GFP}), *Bcl2l11*$^{-/-}$ (*Bim*$^{-/-}$), *Rag2*^{GFP}, *Klf2*^{GFP} and *B2m*$^{-/-}$ mice were described previously[8,9,24,40,41]. *Ifng*^{YFP}, I-Ab$^{-/-}$, *Cd1*$^{-/-}$, *Cd4*^{CreERT2}, *Cd28*$^{-/-}$ and Rosa26^{TdT} (Jax 007914) were obtained from Jackson Laboratories. *Il15*$^{-/-}$ and K^{b}D$^{b-/-}$ mice were obtained from Taconic. *Rag2*$^{-/-}$ mice were obtained from Jackson Laboratories and bred with B6.SJL mice to establish a CD45.1/2^{+} *Rag2*$^{-/-}$ line. For chimeras, lethally irradiated recipients were reconstituted with T cell depleted donor bone marrow cells and provided with neomycin- and proximicin B supplemented water for two weeks. Chimeras were analyzed minimum eight weeks after reconstitution. All animal experiments were approved by the Institutional Animal Care and Use Committee of the University at Minnesota.

IEL isolation

IELs were isolated similarly to a previously published protocol[42]. Changes were made as follows: DTT was used instead of DTE and samples were placed into a 37 °C shaking incubator for 30 min for incubation with the DTT solution. Samples were resuspended in 40% percoll and overlayed onto 80% percoll and spun, and the interlayer was collected and labeled for flow cytometry.

Flow cytometry

Single-cell suspensions of indicated tissues were labeled with antibodies from eBioscience, Biolegend, Tonbo or R&D Systems. Clones: CD4 (RM4-5), CD8α (53-6.7), CD103 (M290), TCRβ (H57-597), CD44 (IM7), H-2K^{b} (AF6-88.5), CD5 (53-7.3), CD25 (PC61), PD-1 (J43), TCRγδ (GL3), CD122 (TM-b1), $\alpha_4\beta_7$ (DATK32), NK1.1 (PK136), T-bet (4B10), V_α2 (B20.1), V_α3.2 (RR3-16), V_β2 (B20.6), V_β3 (KJ25), V_β4 (KT4), V_β5.1/5.2 (MR9-4), V_β6 (PR4-7), V_β9 (MR10-2), Ki-67 (16A8), CCR4 (2G12), CCR7 (4B12), CCR9 (CW-1.2), CXCR3 (CXCR3-173), CXCR4 (L276F12), CD69 (H1.2F3), Qa2 (69HI-9-9), CD45.1 (A20), CD45.2 (104). Biotinylated CD1d/PBS57 monomers were obtained from US National Institutes of Health tetramer facility and incubated with PE, APC or PE/Cy7 Streptavidin to fluorochrome-labeled multimers. Cells were stained for 20 min at 20 °C. When staining for CCR4 or CCR7, the cells were incubated for 30 min at 37 °C. For S1PR1 staining thymic samples were enriched for IELp by depletion of CD4^{+} cells (Miltenyi, manual MACS). Enriched cells were labeled with 10 μg Rat IgG2 anti-mS1PR1 (R&D Systems, clone 713412) per 1 × 10^{6} cells for 30 min at 4 °C. The samples were then labeled with biotin anti-rat IgG (clone G28-5) for 20 min on ice and subsequently incubated with

streaptavidin-fluorochrome. Before staining with other markers, the samples were blocked with 5% rat serum and 1% free streptavidin.

SPADE analysis

Spanning tree analysis was performed using the Cytobank Premium online platform (https://premium.cytobank.org/cytobank/) and according to previous publications[18,19]. Heatmaps were created with the Matrix2png version 1.2.1 online platform (http://www.chibi.ubc.ca/matrix2png/).

Adoptive transfer studies

Pooled thymic single-cell suspensions were enriched for IELp by depletion of $CD8^+$ and/or $CD4^+$ cells by manual MACS (Miltenyi). IELp were then purified by flow cytometry. Within the live $CD25^-CD1dtet^-TCR\gamma\delta^-CCR7^-CD4^-CD8\alpha^-$ population $CD5^+TCR\beta^+$ cells were divided and purified as $CD122^{hi}PD\text{-}1^{hi}$ (type A) or $CD122^{hi}PD\text{-}1^-$ (type B) IELp. Between 50,000 and 280,000 cells were transferred into recipients per i.v. injection. Total DN competitors were purified by MACS-depletion of $CD4^+$ and $CD8^+$ cells (Miltenyi).

Immunofluorescence

Immunofluorescence of *Tbx21*^{GFP} thymi was described previously[17]. Briefly, thymi were incubated overnight in PBS containing PE labeled CD1d-tetramer loaded with PBS57 at 4 °C. Thymi were then washed, fixed with 4% paraformaldehyde (PFA) for 1 h and snap frozen. 5 μm sections were blocked with PBS 5% bovine serum albumin (BSA) and goat serum (Jackson Laboratory) prior to staining. Clone RORg2 was used for RORγτ staining. Processing of *Nr4a1*^{GFP} thymi up until rabbit anti-mouse β5t labeling with the primary antibody was performed as previously described[13] with the exception of using 3 μm sections. Briefly, thymi were fixed in 4% PFA overnight followed by immersion in 15% (wt/vol) sucrose in PBS overnight. Thymi were then frozen. For immunofluorescence, sections were treated with 0.1% Triton-X100/PBS (PBST) for 5 min at 20 °C and then incubated in PBS 3% BSA for 1 h at 20 °C prior to staining. For PD-1 staining, goat anti-mouse PD-1 (R&D Systems, cat. # AF1021) was added with the anti-β5t (MBL, cat. # PD021) for overnight labeling. Secondary antibody staining was done with AF647 donkey anti-rabbit IgG (Jackson ImmunoResearch, cat. # 711-605-152) and AF555 donkey anti-goat IgG (Invitrogen, cat. # A-21432) for 2 h at 20°C prior to DAPI staining. The Sections were then covered with a Prolong anti-fade mounting medium (Life Technologies) and images obtained 1 to 3 days later using a Leica DM6000B Epi-Fluorescent microscope.

Histo-cytometry

Histo-cytometry was performed as described previously[17]. The quantified values represent the frequencies after normalization to the total average cortical and medullary areas as previously described[17].

Intraveneous labeling of cells in the PVS

1 μg PE-conjugated anti-CD45.2 antibody was injected intravenously per mouse and mice were euthanized for tissue collection 3-4 min after injections. Initially, perfused animals

were compared to non-perfused ones. As no significant differences were observed, subsequent analysis was done on non-perfused mice. Labeled cells were isolated from single cell suspensions with anti-PE beads (Miltenyi) and manual MACS prior to further labeling for flow cytometry. Potential contamination of the labeled fraction by cells in circulation is negligible as indicated by reversed proportions of type A or -B like cells in blood (Fig. 5b), as well as the largely different proportions of various cell types (Supplementary Fig. 4c,d), and by different CD8SP/CD4SP or mature IELp/CD4SP ratios (Supplementary Fig. 4e) in the blood.

FTY720 treatment

25 μg FTY720 (Calbiochem) in PBS was injected intraperitoneally for six consecutive days and tissues were harvested on day seven. Mock- and untreated animals were used as controls.

Ultrasound-guided intrathymic injections (RTE Assay)

Intrathymic injections of 10–20 μl EZ-Link Sulfo-NHS biotin (ThermoFisher Scientific) were performed as described previously[43] and using the Vevo 2100 System. Two factors substantiated the accuracy of this method: First, the proportion of streptavidin^{+}B220^{+} cells was less than 5% (Supplementary Fig. 5b). Second, when performed with *Rag2*^{GFP} mice, over 90% of streptavidin^{+} TCRβ^{+} cells were GFP^{+} (Fig. 5c and Supplementary Fig. 5b) indicative of their recent thymic origin.

Time-stamp labeling

Cd4^{CreERT2} mice were bred with Rosa26^{TdT} mice. The offspring was injected intraperitoneally with 2 mg tamoxifen (Sigma-Aldrich) in sunflower oil 2% EtOH on one or two consecutive days. The thymus of tamoxifen recipients was analyzed on various days post injections.

Statistical analysis

Prism 5.0 and 6.0 were used for data analysis and arrangement. For comparison of two datasets, the unpaired two-tailed Student's *t* test was used. For comparison of 3 or more datasets, one way ANOVA with Bonferroni post-test was performed. Details on sample size, experimental replicates and statistics are included in the figure legends.

Data availability statement

The data used to support the conclusions of our study are available from the corresponding author upon request.

Supplementary Material

Refer to Web version on PubMed Central for supplementary material.

Acknowledgments

The authors wish to thank J. Ding and J. Lam for technical assistance. Some results mentioned in the manuscript but not shown were derived from experiments set up by E.R. Breed and H. Wang. We further thank T. Baldwin,

Golec and H. Borges de Silva for reading the manuscript and providing feedback and suggestions. This work was supported by NIH grants R37 AI39560 and PO1 AI35296 to K.A.H., K99 AI114889 to Y.J.L. and T35 AI118620-01 to R.L.K.

References

1. Sheridan BS, Lefrançois L. Intraepithelial lymphocytes: to serve and protect. Curr Gastroenterol Rep. 2010; 12:513–521. DOI: 10.1007/s11894-010-0148-6 [PubMed: 20890736]
2. Cheroutre H, Lambolez F, Mucida D. The light and dark sides of intestinal intraepithelial lymphocytes. Nat Rev Immunol. 2011; 11:445–456. DOI: 10.1038/nri3007 [PubMed: 21681197]
3. Gangadharan D, et al. Identification of pre- and postselection TCRalphabeta+ intraepithelial lymphocyte precursors in the thymus. Immunity. 2006; 25:631–641. DOI: 10.1016/j.immuni.2006.08.018 [PubMed: 17045820]
4. Mayans S, et al. αβT cell receptors expressed by CD4(-)CD8αβ(-) intraepithelial T cells drive their fate into a unique lineage with unusual MHC reactivities. Immunity. 2014; 41:207–218. DOI: 10.1016/j.immuni.2014.07.010 [PubMed: 25131531]
5. McDonald BD, Bunker JJ, Ishizuka IE, Jabri B, Bendelac A. Elevated T cell receptor signaling identifies a thymic precursor to the TCRαβ(+)CD4(-)CD8β(-) intraepithelial lymphocyte lineage. Immunity. 2014; 41:219–229. DOI: 10.1016/j.immuni.2014.07.008 [PubMed: 25131532]
6. Klose CS, et al. The transcription factor T-bet is induced by IL-15 and thymic agonist selection and controls CD8αα(+) intraepithelial lymphocyte development. Immunity. 2014; 41:230–243. DOI: 10.1016/j.immuni.2014.06.018 [PubMed: 25148024]
7. Guo X, Tanaka Y, Kondo M. Thymic precursors of TCRαβ(+)CD8αα(+) intraepithelial lymphocytes are negative for CD103. Immunol Lett. 2015; 163:40–48. DOI: 10.1016/j.imlet.2014.11.007 [PubMed: 25448708]
8. Lee YJ, Holzapfel KL, Zhu J, Jameson SC, Hogquist KA. Steady-state production of IL-4 modulates immunity in mouse strains and is determined by lineage diversity of iNKT cells. Nat Immunol. 2013; 14:1146–1154. DOI: 10.1038/ni.2731 [PubMed: 24097110]
9. Xing Y, Wang X, Jameson SC, Hogquist KA. Late stages of T cell maturation in the thymus involve NF-κB and tonic type I interferon signaling. Nat Immunol. 2016; 17:565–573. DOI: 10.1038/ni.3419 [PubMed: 27043411]
10. Sanjo H, Tokumaru S, Akira S, Taki S. Conditional Deletion of TAK1 in T Cells Reveals a Pivotal Role of TCRαβ+ Intraepithelial Lymphocytes in Preventing Lymphopenia-Associated Colitis. PLoS One. 2015; 10:e0128761. [PubMed: 26132627]
11. Pobezinsky LA, et al. Clonal deletion and the fate of autoreactive thymocytes that survive negative selection. Nat Immunol. 2012; 13:569–578. DOI: 10.1038/ni.2292 [PubMed: 22544394]
12. Stritesky GL, Hogquist KA. Death diverted, but to what? Nat Immunol. 2012; 13:528–530. DOI: 10.1038/ni.2311 [PubMed: 22610242]
13. Stritesky GL, et al. Murine thymic selection quantified using a unique method to capture deleted T cells. Proc Natl Acad Sci U S A. 2013; 110:4679–4684. DOI: 10.1073/pnas.1217532110 [PubMed: 23487759]
14. Berlin C, et al. Alpha 4 beta 7 integrin mediates lymphocyte binding to the mucosal vascular addressin MAdCAM-1. Cell. 1993; 74:185–195. [PubMed: 7687523]
15. Hamann A, Andrew DP, Jablonski-Westrich D, Holzmann B, Butcher EC. Role of alpha 4-integrins in lymphocyte homing to mucosal tissues in vivo. J Immunol. 1994; 152:3282–3293. [PubMed: 7511642]
16. Schön MP, et al. Mucosal T lymphocyte numbers are selectively reduced in integrin alpha E (CD103)-deficient mice. J Immunol. 1999; 162:6641–6649. [PubMed: 10352281]
17. Lee YJ, et al. Tissue-Specific Distribution of iNKT Cells Impacts Their Cytokine Response. Immunity. 2015; 43:566–578. DOI: 10.1016/j.immuni.2015.06.025 [PubMed: 26362265]
18. Bendall SC, et al. Single-cell mass cytometry of differential immune and drug responses across a human hematopoietic continuum. Science. 2011; 332:687–696. DOI: 10.1126/science.1198704 [PubMed: 21551058]

19. Qiu P, et al. Extracting a cellular hierarchy from high-dimensional cytometry data with SPADE. Nat Biotechnol. 2011; 29:886–891. DOI: 10.1038/nbt.1991 [PubMed: 21964415]
20. Kwan J, Killeen N. CCR7 directs the migration of thymocytes into the thymic medulla. J Immunol. 2004; 172:3999–4007. [PubMed: 15034011]
21. Ueno T, et al. CCR7 signals are essential for cortex-medulla migration of developing thymocytes. J Exp Med. 2004; 200:493–505. DOI: 10.1084/jem.20040643 [PubMed: 15302902]
22. Fan X, Rudensky AY. Hallmarks of Tissue-Resident Lymphocytes. Cell. 2016; 164:1198–1211. DOI: 10.1016/j.cell.2016.02.048 [PubMed: 26967286]
23. Boursalian TE, Golob J, Soper DM, Cooper CJ, Fink PJ. Continued maturation of thymic emigrants in the periphery. Nat Immunol. 2004; 5:418–425. DOI: 10.1038/ni1049 [PubMed: 14991052]
24. McCaughtry TM, Wilken MS, Hogquist KA. Thymic emigration revisited. J Exp Med. 2007; 204:2513–2520. DOI: 10.1084/jem.20070601 [PubMed: 17908937]
25. Uehara S, Song K, Farber JM, Love PE. Characterization of CCR9 expression and CCL25/thymus-expressed chemokine responsiveness during T cell development: CD3(high)CD69+ thymocytes and gammadeltaTCR+ thymocytes preferentially respond to CCL25. J Immunol. 2002; 168:134–142. [PubMed: 11751956]
26. Misslitz A, et al. Thymic T cell development and progenitor localization depend on CCR7. J Exp Med. 2004; 200:481–491. DOI: 10.1084/jem.20040383 [PubMed: 15302903]
27. Plotkin J, Prockop SE, Lepique A, Petrie HT. Critical role for CXCR4 signaling in progenitor localization and T cell differentiation in the postnatal thymus. J Immunol. 2003; 171:4521–4527. [PubMed: 14568925]
28. Hu Z, Lancaster JN, Sasiponganan C, Ehrlich LI. CCR4 promotes medullary entry and thymocyte-dendritic cell interactions required for central tolerance. J Exp Med. 2015; 212:1947–1965. DOI: 10.1084/jem.20150178 [PubMed: 26417005]
29. Drennan MB, et al. Cutting edge: the chemokine receptor CXCR3 retains invariant NK T cells in the thymus. J Immunol. 2009; 183:2213–2216. DOI: 10.4049/jimmunol.0901213 [PubMed: 19620294]
30. Gerner MY, Kastenmuller W, Ifrim I, Kabat J, Germain RN. Histo-cytometry: a method for highly multiplex quantitative tissue imaging analysis applied to dendritic cell subset microanatomy in lymph nodes. Immunity. 2012; 37:364–376. DOI: 10.1016/j.immuni.2012.07.011 [PubMed: 22863836]
31. Steinert EM, et al. Quantifying Memory CD8 T Cells Reveals Regionalization of Immunosurveillance. Cell. 2015; 161:737–749. DOI: 10.1016/j.cell.2015.03.031 [PubMed: 25957682]
32. White AJ, et al. An essential role for medullary thymic epithelial cells during the intrathymic development of invariant NKT cells. J Immunol. 2014; 192:2659–2666. DOI: 10.4049/jimmunol.1303057 [PubMed: 24510964]
33. Matloubian M, et al. Lymphocyte egress from thymus and peripheral lymphoid organs is dependent on S1P receptor 1. Nature. 2004; 427:355–360. DOI: 10.1038/nature02284 [PubMed: 14737169]
34. Carlson CM, et al. Kruppel-like factor 2 regulates thymocyte and T-cell migration. Nature. 2006; 442:299–302. DOI: 10.1038/nature04882 [PubMed: 16855590]
35. Odumade OA, Weinreich MA, Jameson SC, Hogquist KA. Krüppel-like factor 2 regulates trafficking and homeostasis of gammadelta T cells. J Immunol. 2010; 184:6060–6066. DOI: 10.4049/jimmunol.1000511 [PubMed: 20427763]
36. Zachariah MA, Cyster JG. Neural crest-derived pericytes promote egress of mature thymocytes at the corticomedullary junction. Science. 2010; 328:1129–1135. DOI: 10.1126/science.1188222 [PubMed: 20413455]
37. Fujiura Y, et al. Development of CD8 alpha alpha+ intestinal intraepithelial T cells in beta 2-microglobulin- and/or TAP1-deficient mice. J Immunol. 1996; 156:2710–2715. [PubMed: 8609387]
38. Ma LJ, Acero LF, Zal T, Schluns KS. Trans-presentation of IL-15 by intestinal epithelial cells drives development of CD8alphaalpha IELs. J Immunol. 2009; 183:1044–1054. DOI: 10.4049/jimmunol.0900420 [PubMed: 19553528]

39. Kunisawa J, et al. et al. Sphingosine 1-phosphate dependence in the regulation of lymphocyte trafficking to the gut epithelium. J Exp Med. 2007; 204:2335–2348. DOI: 10.1084/jem.20062446 [PubMed: 17875673]

40. Moran AE, et al. T cell receptor signal strength in Treg and iNKT cell development demonstrated by a novel fluorescent reporter mouse. J Exp Med. 2011; 208:1279–1289. DOI: 10.1084/jem.20110308 [PubMed: 21606508]

41. Weinreich MA, et al. KLF2 transcription-factor deficiency in T cells results in unrestrained cytokine production and upregulation of bystander chemokine receptors. Immunity. 2009; 31:122–130. DOI: 10.1016/j.immuni.2009.05.011 [PubMed: 19592277]

42. Lefrançois L, Lycke N. Isolation of mouse small intestinal intraepithelial lymphocytes, Peyer's patch, and lamina propria cells. Curr Protoc Immunol. 2001; Chapter 3(Unit 3.19)

43. Blair-Handon R, Mueller K, Hoogstraten-Miller S. An alternative method for intrathymic injections in mice. Lab Anim (NY). 2010; 39:248–252. DOI: 10.1038/laban0810-248 [PubMed: 20664574]

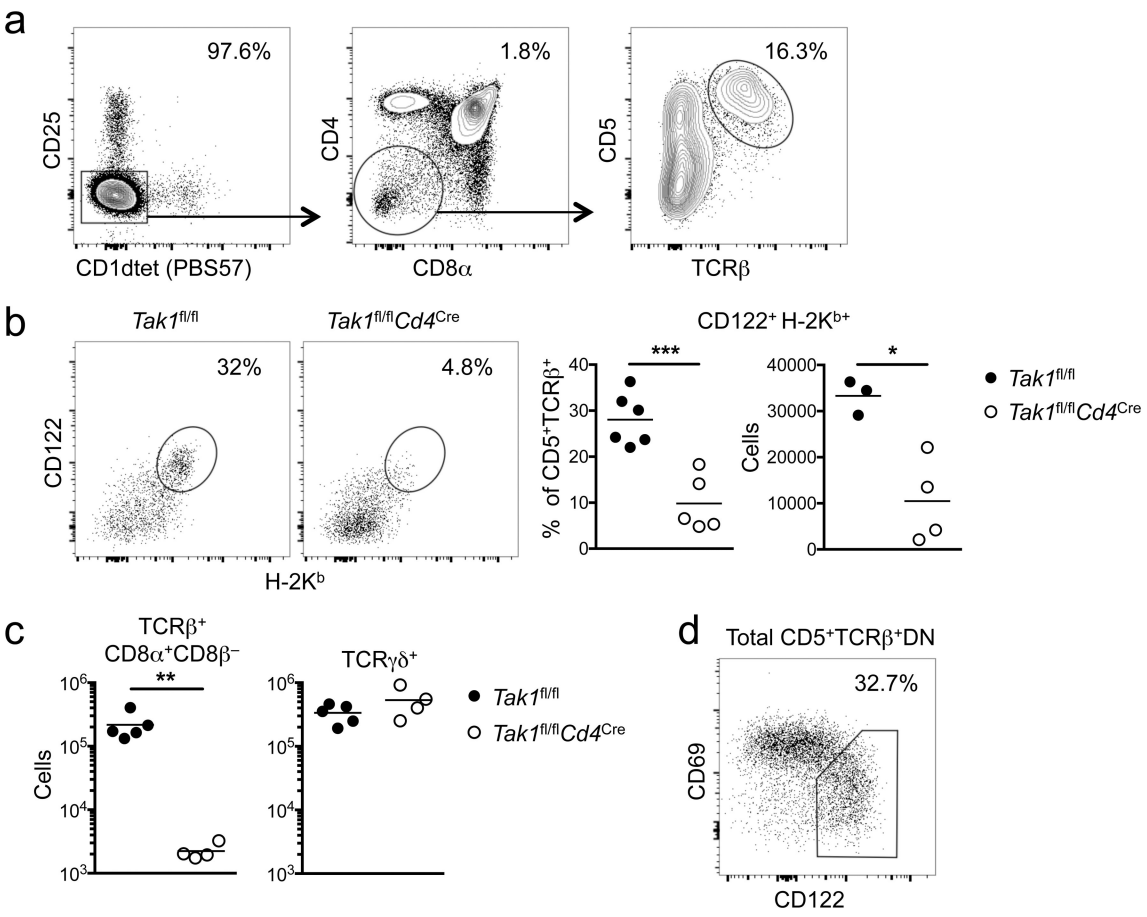

Figure 1. A Subset of TCRβ$^+$DN Cells Is Phenotypically and Functionally Mature

(**a**) Flow cytometric identification of TCRβ$^+$ DN cells in the thymus. (**b**) Within thymic TCRβ$^+$ DN cells of *Tak1*$^{fl/fl}$ or *Tak1*$^{fl/fl}$*Cd4*^{Cre} mice, proportions and numbers of mature CD122$^+$H-2K^{b+} cells were determined. (**c**) Numbers of CD8αα and TCRγδ$^+$ IELs were determined from *Tak1*$^{fl/fl}$ or *Tak1*$^{fl/fl}$*Cd4*^{Cre} small intestines by flow cytometry. (**d**) CD69 and CD122 expression on thymic wild-type TCRβ$^+$ DN cells. Dot plots are representative of more than 10 experiments (**a**), 3 experiments with 6 (*Tak1*$^{fl/fl}$) or 5 (*Tak1*$^{fl/fl}$*Cd4*^{Cre}) mice (**b**), or 2 experiments with 3 mice (**d**). Graphs show combined data from 3 (b, left graph and c) or 2 (b, right graph) independent experiments with each symbol representing an individual mouse. *$P < 0.05$, *** $P < 0.001$, Student's t test. Horizontal lines in graphs indicate the mean.

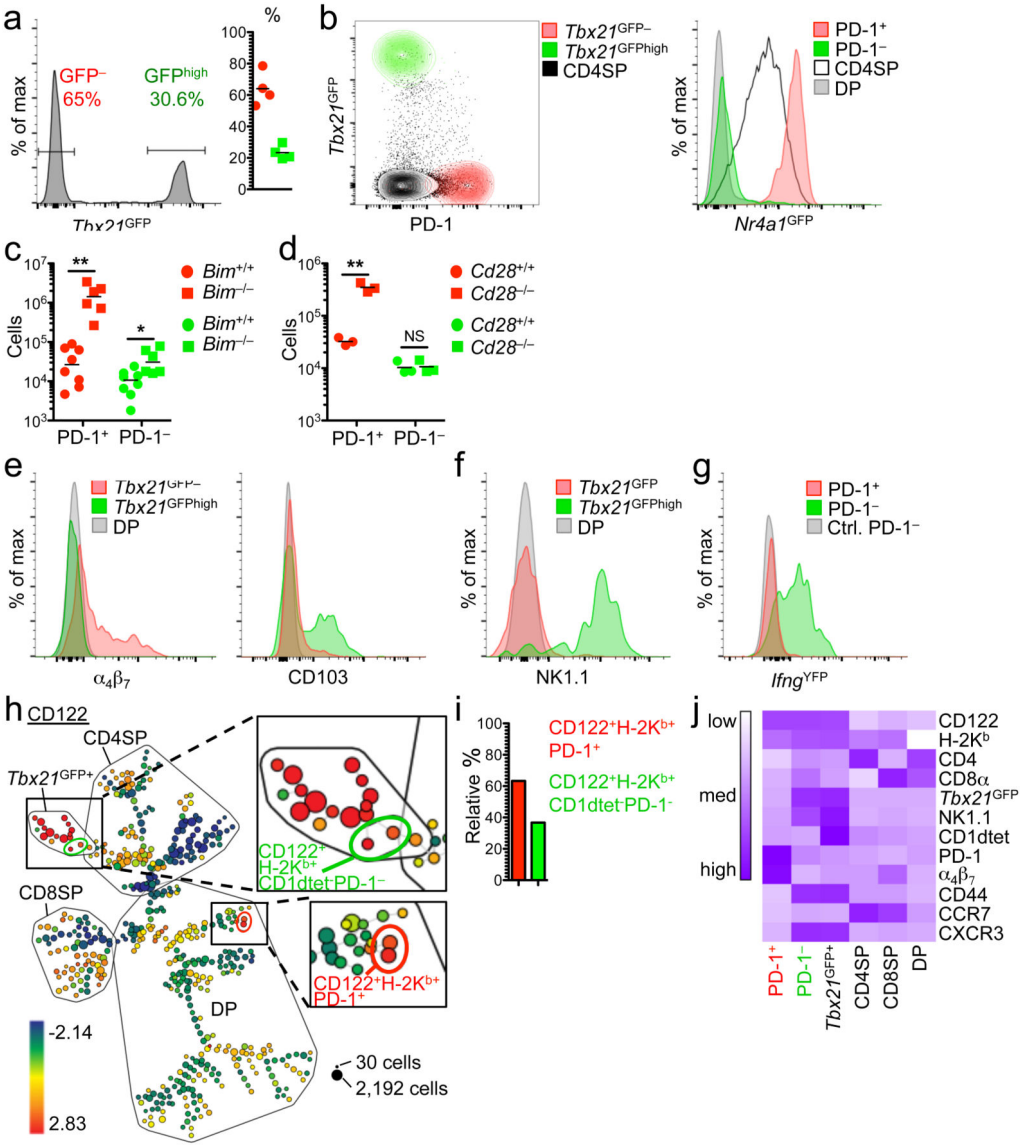

Figure 2. Mature TCRβ$^+$DN Cells Divide into Two Major Subsets

(**a**) TCRβ$^+$ DN thymocytes were analyzed for GFP expression in *Tbx21*^{GFP} (T-bet-GFP) mice. (**b**) PD-1 surface staining of *Tbx21*^{GFPhigh} (green) or *Tbx21*$^{GFP–}$ (red) TCRβ$^+$DN thymocytes, and Nur77-GFP expression of PD-1$^+$ or PD-1$^–$ TCRβ$^+$DN cells in *Nr4a1*^{GFP}. Controls: CD4SP and DP. (**c**) Graphical representation of PD-1$^+$ (red) and PD-1$^–$ or PD-1$^–$NK1.1$^+$ (green) total cell numbers within the thymic TCRβ$^+$ DN population of wild-type (WT) or *Bim*$^{–/–}$ mice. (**d**) Cumulative data of PD-1$^+$ (red) and PD-1$^–$ (green) total cell numbers within the thymic TCRβ$^+$DN population of WT or *Cd28*$^{–/–}$ mice. (**e** and **f**) Expression of α4β7 and CD103 (**e**), or NK1.1 (**f**) by *Tbx21*$^{GFP+}$ (green) or *Tbx21*$^{GFP–}$ (red) TCRβ$^+$ DN. (**g**) YFP expression by PD-1$^+$ (red) and PD-1$^–$ (green) TCRβ$^+$DN of *Ifng*^{YFP} or WT control mice. (**h**–**j**) SPADE analysis of flow cytometric data, gated on CD5$^+$TCRβ$^+$ thymocytes as shown in Supplementary Fig. 1a. Individual bubbles in (**h**) show populations determined by expression of markers as shown in (**j**) and Supplementary Fig. 1. The color of

individual nodes indicates median intensity of CD122, node size indicates cell number. $CD122^{+}H\text{-}2K^{b+}PD\text{-}1^{+}$ type A and $CD122^{+}H\text{-}2K^{b+}CD1dtet^{-}PD\text{-}1^{-}$ type B IELp in (**h**–**j**) are encircled and/or labeled in red or green, respectively. Percentages of type A (red) and type B (green) IELp relative to each other are shown in (**i**). Median intensities of markers in Supplementary Fig. 1 are represented as a heatmap (**j**). Dot plots and histograms shown in (**a**–**g**) are representative for 3 experiments. Graphs are pooled from 4 experiments with (**a**), 4 experiments (**c**), or 1 experiment (**d**) with each symbol representing an individual mouse. * $P < 0.05$, ** $P < 0.01$, Student's *t* test. Horizontal lines in graphs indicate the mean.

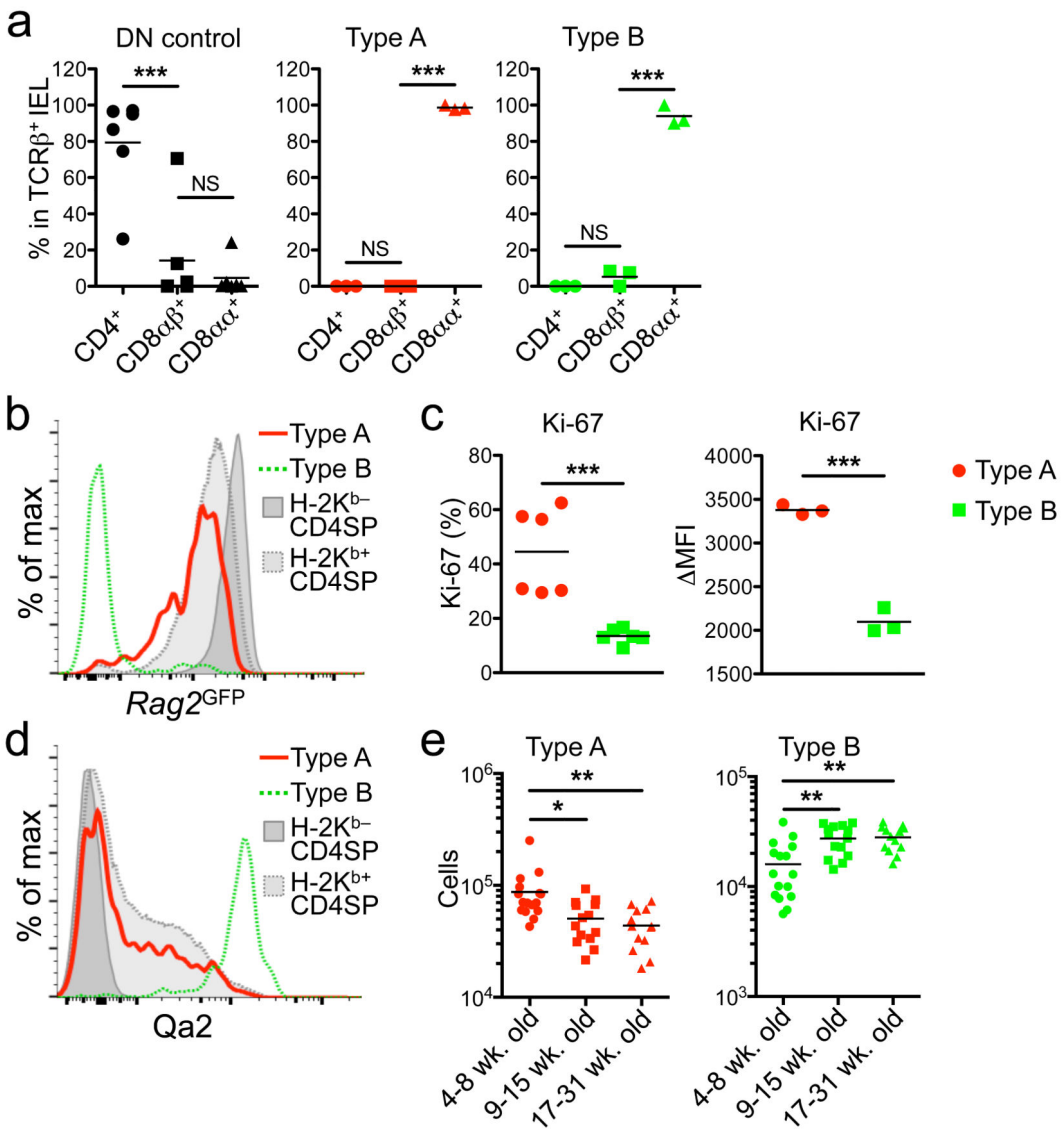

Figure 3. Both PD-1$^+$ "Type A" and PD-1$^-$ "Type B" Cells Give Rise to CD8αα IEL

(**a**): Purified type A (red) or B (green) IELp (sorted as described in the Methods section) were transferred alongside total DN control cells into *Rag2*$^{-/-}$ recipients. Transferred cells were recovered from the small intestinal IEL compartment 5-10 weeks after transfer. Graphs show recovered cells as the proportion of CD4$^+$, CD8αβ$^+$ or CD8αα$^+$ cells within TCRβ$^+$ IELs. (**b**) GFP expression in type A (PD-1$^+$, open, solid red) or B (PD-1$^-$, open, dashed green) IELp, and in H-2K^{b-} (filled, solid) or H-2K^{b+} (filled, dashed) CD4SP from *Rag2*^{GFP} mice. (**c**) Type A (PD-1$^+$, red) or B (PD-1$^-$T-bet$^+$, green) IELp were stained for Ki-67. Graphs show the percent (left graph) and MFI minus the negative control's MFI (right graph). (**d**) Qa2 expression by type A (PD-1$^+$, open, solid red) or B (PD-1$^-$, open, dashed green) IELp, and in H-2K^{b-} (filled, solid) or H-2K^{b+} (filled, dashed) CD4SP. (**e**) Number of type A (PD-1$^+$, red) or B (PD-1$^-$NK1.1$^+$, green) IELp from mice within different age groups as indicated. Histograms are representative of 3 independent experiments. Graphs in (**a**) are combined from 3 experiments. (**c**) shows graphs pooled from 2 experiments (left) or 1

experiment representative for 2 experiments (right). Graphs in (**e**) are combined from 3 experiments. Each symbol in graphs represents an individual mouse. * $P < 0.05$, ** $P < 0.01$, *** $P < 0.001$, Student's *t* test (**c**) or ANOVA with Bonferroni post-test (**a**, **e**). Horizontal lines in graphs indicate the mean.

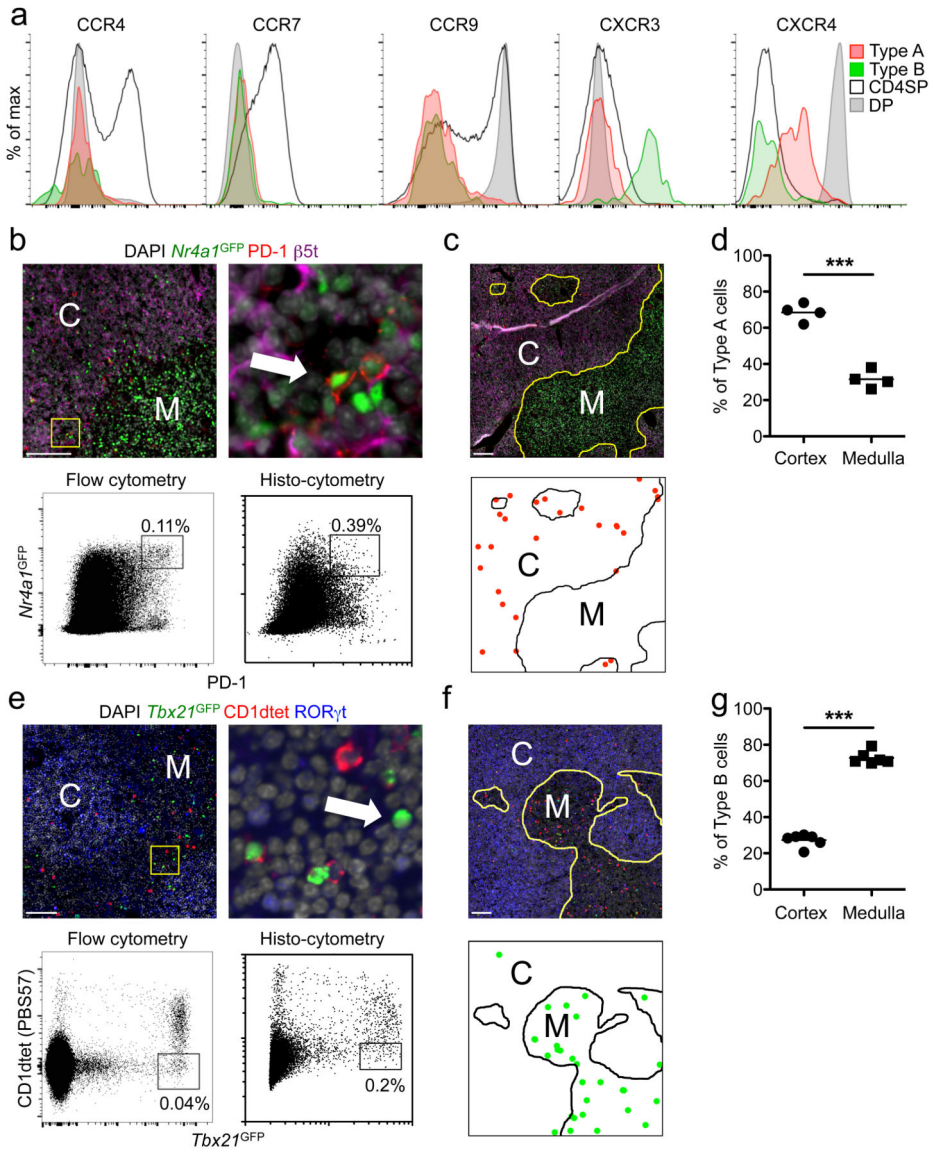

Figure 4. Thymic Localization of Type A and B IELp

(**a**) Type A (PD-1^{+}, red) and B (PD-1, green) IELp as well as CD4SP and DP thymocytes were stained for the indicated chemokine receptors and analyzed by flow cytometry. Histograms are representative of 3 individual mice in 2 experiments. (**b**–**d**) Thymic sections of *Nr4a1*^{GFP} mice were stained with PD-1, β5t and DAPI (red, purple and grey, respectively, **b**, **c**). The arrow in (**b**) indicates a GFP^{high}PD-1^{+} type A IELp. Dot plots in (**b**) represent histo-cytometric analysis (right) of immunofluorescence images in comparison to flow cytometric analysis (left). (**c**, bottom) shows localization of type A IELp (red dots) as determined by histo-cytometry. (**d**) Cortical and medullary frequencies were analyzed and pooled from images of 3 mice with each symbol representing an individual image area. C, cortex; M, medulla. Scale bars 100 μm. (**e**–**g**) Analysis of type B IELp like in (**b**–**d**). *Tbx21*^{GFP} thymic sections were stained with CD1dtet, RORγt and DAPI (red, blue and grey, respectively, **e**, **f**), type B IELp were determined as GFP^{high}CD1dtet^{-} cells (arrow, **e**). Type B

IELp in (**f**, bottom) are indicated as green dots. (**g**) Cortical and medullary frequencies were analyzed and pooled from images of 3 mice with each symbol representing an individual image area. *** $P < 0.001$, Student's *t* test.

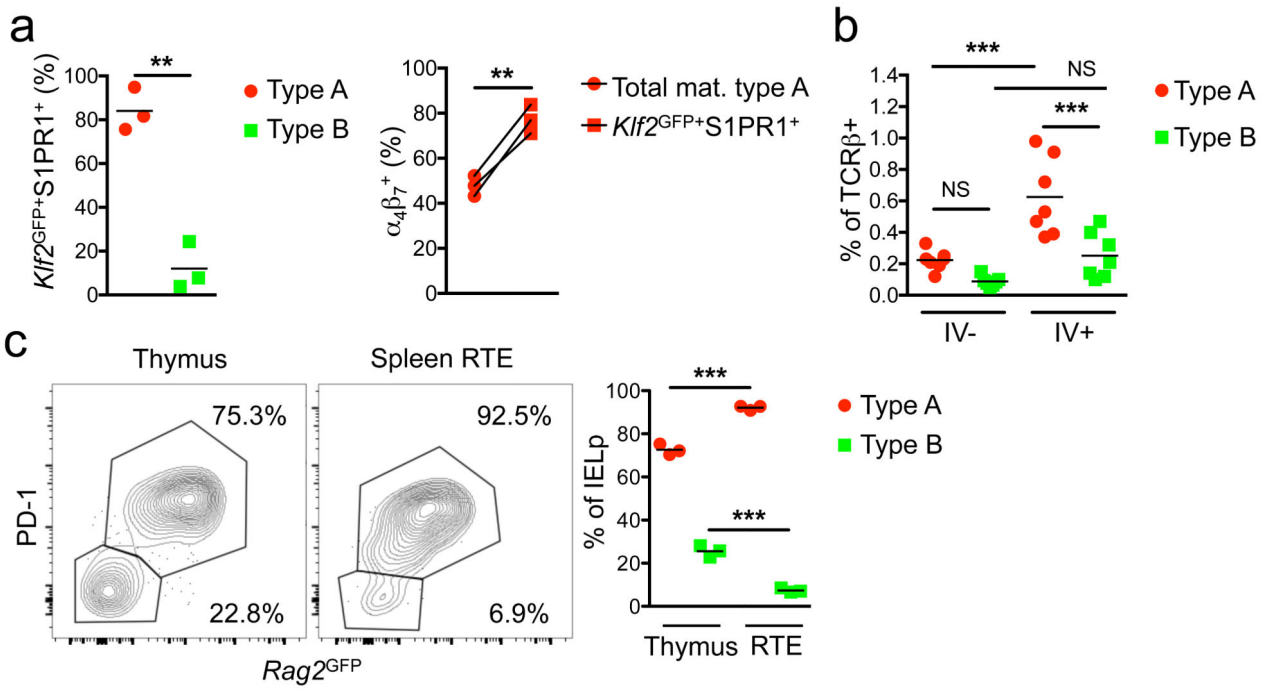

Figure 5. Emigration of Type A IELp Is Dominant over Type B

(**a**) IELp from *Klf2*^{GFP} mice were further stained for S1PR1 (Supplementary Fig. 4a). Left: percent type A (PD-1^{+}, red) or B (PD-1^{-}, green) cells within *Klf2*$^{+}$S1PR1^{+} mature IELp. Right: Percent $\alpha_4\beta_7^{+}$ cells in the whole mature type A IELp population versus *Klf2*$^{+}$S1PR1^{+} mature type A IELp. (**b**) Mice were intravenously labeled with anti-CD45.2 PE (Supplementary Fig. 4c). Shown are the proportions of type A (PD-1^{+}, red) or B (PD-1^{-}, green) mature phenotype cells within the unlabeled (IV–) and labeled (IV+) thymic fractions. (**c**) *Rag2*^{GFP} mice were intrathymically injected with NZ-Link Sulfo-NHS-Biotin and analyzed 24h later. Shown are type A (PD-1^{+}, red) and B (PD-1^{-}, green) cells within mature IELp of the streptavidin-labeled fraction. Graphs in (**a**) and (**b**) are combined from 3 (**a**) or 5 (**b**) independent experiments. (**c**): plots are representative for and graph is combined from 3 mice in one experiment. Another two independent experiments with C57BL/6 mice showed similar results. All graphs indicate the mean and each symbol represents an individual mouse. ** $P < 0.01$, *** $P < 0.001$, Student's *t* test (**a**) or ANOVA with Bonferroni post-test (**b**, **c**).

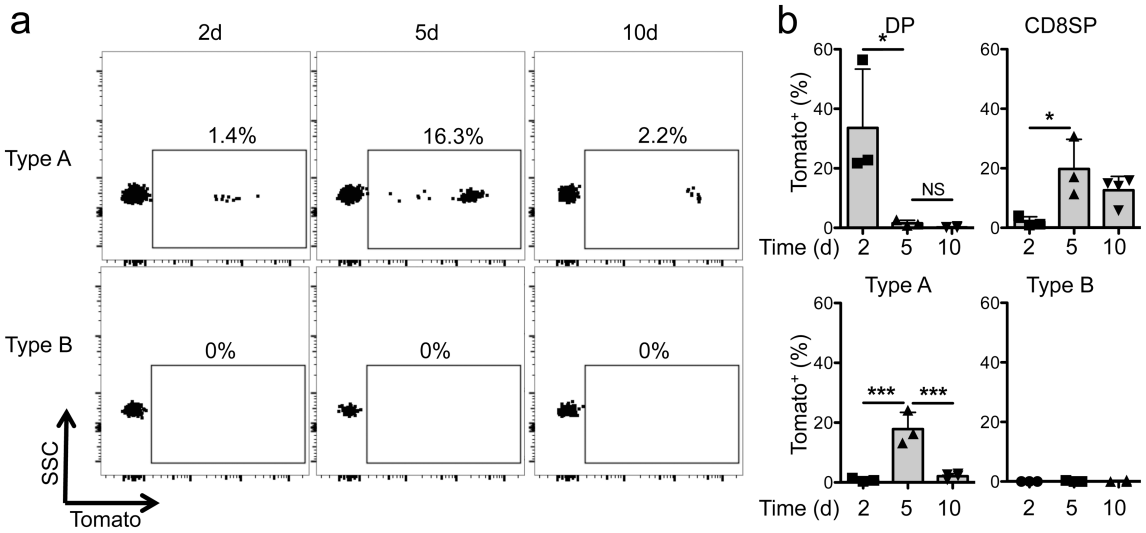

Figure 6. No Immediate Precursor-Product Relationship Between Type A and B IELp

Cd4^{CreERT2} and Rosa26^{TdT} mice were crossed and the offspring was injected with tamoxifen. Thymic populations were analyzed for tdTomato protein expression on day 2, 5 or 10 after tamoxifen exposure. Shown are representative plots (a) and cumulative data of indicated populations (b). Type A and B IELp were pre-gated on mature phenotype IELp and defined as PD-1^{+} or PD-1^{-}NK1.1^{+}, respectively. Cumulative data of 3 experiments with 3 (2d, 4d) or 4 (10d) mice. * $P < 0.05$, ***p < 0.001, ANOVA with Bonferroni post-test. Graphs show mean (± s.d.).

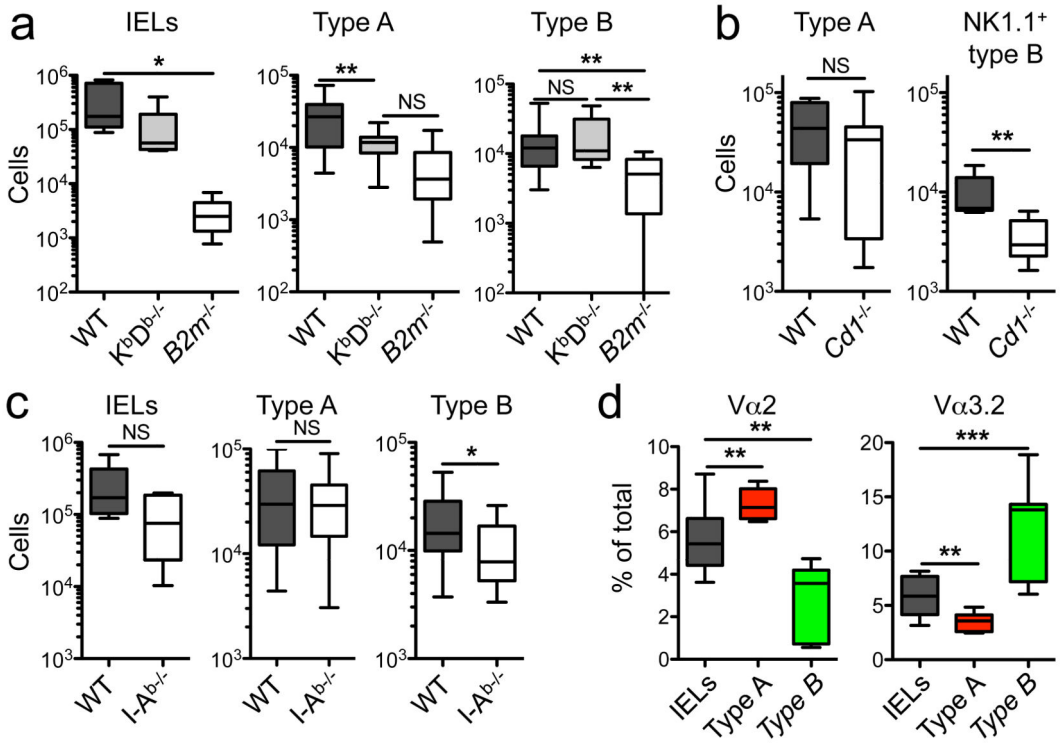

Figure 7. Type A and B IELp Have Different Antigen-Receptor Specificities

(**a**) Absolute numbers of CD8αα IELs and type A (PD-1$^+$) or B (PD-1$^-$) IELp and in classical MHC class-I and in β2m deficient models. Due to the lack of H-2K^b, mature IELp were defined by CD122 expression only. (**b**) PD-1$^+$ type A and PD-1$^-$NK1.1$^+$ type B IELp numbers were analyzed in WT versus CD1d-deficient thymi. (**c**) Graphs show absolute numbers of CD8αα IELs and type A (PD-1$^+$) or B (PD-1$^-$) IELp in MHC class-II deficient mice. (**d**) TCR V_α analysis of type A (PD-1$^+$, red) and B (PD-1$^-$, green) IELp, and CD8αα IELs. Graphs are combined from 6 experiments with 6 (WT, K^{b}D$^{b-/-}$) and 7 (*B2m*$^{-/-}$) mice (**a**, IELs), 11 experiments with 27 (WT), 12 (K^{b}D$^{b-/-}$) and 20 (*B2m*$^{-/-}$) mice (**a**, type A and B), 4 experiments with 5 (WT) and 9 (*Cd1*$^{-/-}$) mice (**b**), 5 experiments with 5 (WT) and 7 (I-A$^{b-/-}$) mice (**c**, IELs), 10 experiments with 27 (WT) and 14 (I-A$^{b-/-}$) mice (**c**, type A and B), 11 experiments with 15 mice (**d**, IELs) or 7 experiments with 7 mice (**d**, type A and B). * $P < 0.05$, ** $P < 0.01$, *** $P < 0.001$, ANOVA with Bonferroni post-test (**a**) or Student's *t* test (**b, c** and **d**). All graphs show median (center lines) with 25th and 75th percentiles (box limits). The whiskers indicate the smallest and largest values.